

GAMMA-RAY LIGHT CURVES FROM PULSAR MAGNETOSPHERES WITH FINITE CONDUCTIVITY

Constantinos Kalapotharakos^{1,2}, Alice K. Harding², Demosthenes Kazanas²
and Ioannis Contopoulos³

¹*University of Maryland, College Park (UMDCP/CRESST), College Park, MD 20742, USA;*

²*Astrophysics Science Division, NASA/Goddard Space Flight Center, Greenbelt, MD 20771, USA;*

³*Research Center for Astronomy and Applied Mathematics, Academy of Athens, Athens 11527, Greece;*
constantinos.kalapotharakos@nasa.gov

ABSTRACT

We investigate the shapes of γ -ray pulsar light curves using 3D pulsar magnetosphere models of finite conductivity. These models, covering the entire spectrum of solutions between vacuum and force-free magnetospheres, for the first time afford mapping the GeV emission of more realistic, dissipative pulsar magnetospheres. To this end we generate model light curves following two different approaches: (a) We employ the emission patterns of the slot and outer gap models in the field geometries of magnetospheres with different conductivity σ . (b) We define realistic trajectories of radiating particles in magnetospheres of different σ and compute their Lorentz factor under the influence of magnetospheric electric fields and curvature radiation-reaction; with these at hand we then calculate the emitted radiation intensity. The light curves resulting from these prescriptions are quite sensitive to the value of σ , especially in the second approach. While still not self-consistent, these results are a step forward in understanding the physics of pulsar γ -radiation.

Subject headings: pulsars: general—stars: neutron—Gamma rays: stars

1. INTRODUCTION

The *Fermi* Gamma-Ray Space Telescope has had a major impact on our understanding of pulsar physics with the discovery of over 100 γ -ray pulsars comprising three populations:

young radio-loud pulsars, young radio-quiet pulsars and millisecond pulsars (Abdo et al. 2010). Studying γ -ray pulsars with such a broad range of underlying physical parameters offers an opportunity of deeper understanding the physics underlying the pulsar γ -ray emission and magnetic field geometry. A major issue resolved early in the *Fermi* mission was the site of the pulsar high-energy (GeV) emission. The cutoff of the Vela pulsar phase-averaged spectrum measured by the Fermi Large Area Telescope (LAT) (Abdo et al. 2009) ruled out at high significance the super-exponential shape of magnetic pair production attenuation in polar cap cascades and established the location of the γ -ray emission and particle acceleration in the outer magnetosphere.

Present models for pulsar high-energy emission assume a vacuum retarded dipole (VRD) (Deutsch 1955) field geometry, which is expedient but fundamentally inconsistent. Such models nevertheless have had some success in modeling Fermi pulsar light curves (LCs). Outer Gap (OG) (Cheng et al. 1986; Romani & Yadigaroglu 1995; Hirotani 2008) and Slot Gap (SG) (Muslimov & Harding 2004) models both derive regions of E_{\parallel} bordering the last open field-lines extending to the light-cylinder. The particles accelerating in these ‘gaps’ produce curvature radiation (CR) and inverse-Compton emission, with their Lorentz factors limited by CR reaction forces that balance E_{\parallel} . The pattern of emission on the sky shows caustics that form on the trailing edge of the open field region of each magnetic pole as phase shifts due to dipole geometry, time-of-flight and aberration nearly cancel, and photons from a large range of altitudes arrive in phase (Morini 1983; Dyks & Rudak 2003). Observers viewing at angles crossing the caustics will see one or two narrow peaks that resemble the γ -ray LCs seen by Fermi. Because the GeV emission in these models takes place in a region near the pulsar last open field-lines, the shape of the model LCs is sensitive to, and thus a good diagnostic of, the geometry of the pulsar magnetosphere near the light-cylinder.

Fortunately, this can now be addressed in detail, thanks to recent advances in numerical simulation of pulsar magnetospheres that model the high-altitude field structure critical to the high-energy emission. The global structure of realistic pulsar magnetospheres remains an unsolved problem. Until recently, pulsar LC modeling has employed the magnetospheric geometries of VRD and force-free-electrodynamics (FFE) (Contopoulos et al. 1999; Spitkovsky 2006; Timokhin 2006; Kalapotharakos & Contopoulos 2009). The effects of acceleration fields (Hirotani 2007, 2008) and open-zone currents (Romani & Watters 2010) on the LC have been explored, but these models are not fully self-consistent. In all these models, the sweepback of the magnetic field-lines near the light-cylinder, due to retardation and currents, causes an offset of the polar cap (PC) (and of the entire magnetosphere) in the direction opposite to the rotation, which can affect the γ -ray LCs. Bai & Spitkovsky (2010) modeled γ -ray LCs in FFE field geometry injecting photons along tangents to the field direction of the separatrix. Contopoulos & Kalapotharakos (2010) injected photons only in regions of

the FFE magnetosphere with $J/\rho c = 1$, where J is the current and ρ is the local charge density, as in these regions the electron velocities are expected to be sufficiently close to c to lead to GeV photon production. More recently, Harding et al. (2011) assumed SG geometry to produce model LCs for the VRD and FFE magnetospheres, concluding that the VRD geometry provides better fits to the observed LCs than the FFE geometry. The FFE models present larger field-line sweepback and consequently the corresponding LCs have larger phase-lags relative to the radio pulse which is not consistent with that of observed *Fermi* LCs.

Most recently, resistive magnetosphere models have appeared in the literature (Kalapotharakos et al. 2012 (K12, hereafter); Li et al. 2012), that drop the ideal-MHD requirement in favor of an Ohm’s Law that relates the current to the E and B fields through a finite conductivity. These simulations reveal a range of magnetic field structures, current distributions and spin-down power that lie between the VRD and the FFE solution. Most importantly, models of finite conductivity possess regions of E_{\parallel} which are potential locations of high-energy emission.

In this Letter, we explore for the first time the high-energy emission that is generated in resistive magnetospheres, using their magnetic field structure and E_{\parallel} to produce γ -ray LCs following two different approaches. First, we assume the emission geometry of the SG and OG models and compute the resulting LCs for different values of conductivity to compare with those of the VRD and FFE geometries. In the second approach, we define approximate particle trajectories, and we calculate the corresponding energies (including radiation losses) and CR emission. While neither of these approaches is self-consistent, in that particle motions should affect the fields, they are an important first step in relating the field structure and acceleration dictated by global magnetosphere solutions to observations.

2. LIGHT CURVE MODELING

2.1. Pulsar Magnetosphere Models with Finite Conductivity

Dissipative magnetospheres are necessary for modeling pulsar LCs considering that neither the VRD nor the FFE solutions are compatible with the emission of radiation: The VRD solutions provide maximum accelerating field, E_{\parallel} , but no charges ($\rho = 0$), while the FFE solutions have a sufficiently large number of particles to guarantee the nulling of E_{\parallel} . Herein, we use the dissipative solutions presented recently by K12, which use a phenomenological conductivity σ (*in lieu* of microphysical processes) to relate the current density \mathbf{J} to the fields \mathbf{E} , \mathbf{B} . Although these solutions are still not self-consistent, they are an improvement

over those of VRD and FFE because, besides the global field geometry, they also provide the distribution of E_{\parallel} , a quantity necessary to compute the acceleration of radiating charges.

In the next sections we present model LCs using the structure of magnetic and electric fields provided by dissipative solutions of the perpendicular rotator ($\alpha = 90^\circ$) which span the entire solution space from VRD to FFE. These solutions are presented in detail in K12 and have been produced adopting a very simple prescription for the current density

$$\mathbf{J} = c\rho\frac{\mathbf{E} \times \mathbf{B}}{B^2} + \sigma\mathbf{E}_{\parallel} \quad (1)$$

In this case the current density consists of two components, namely a drift current and a component parallel to the magnetic field. While some simulations explored models with a spatially dependent σ , in this paper we will use only those with constant σ . As σ goes from 0 to ∞ the corresponding solution ranges from VRD to FFE. The solutions we consider here correspond to $\sigma \approx 0.08, 1.5$ and 24Ω , where Ω is the angular frequency of the star. The field structure of the solutions for $\sigma \approx 1.5\Omega$ and $\sigma \approx 24\Omega$ are shown in the last rows of figures 4 and 3 of K12, respectively.

2.2. Geometric Approach

A simple method of generating pulsar LCs, used in many previous studies (e.g Dyks & Harding 2004; Watters et al. 2009; Venter et al. 2009), adopts the geometry of physical emission models that have computed the shape of accelerator gaps with assumed field structure and sources of charge. This method can directly compare LCs from magnetospheres having finite conductivity with LCs in VRD and FFE magnetospheres. To explore how the magnetic field structure and offset PCs influence γ -ray pulsar LCs, we have generated model LCs using a geometrical version of the SG and OG models (e.g. Dyks & Harding 2004; Watters et al. 2009; Venter et al. 2009). The SG has its origin in PC pair cascades that screen the accelerating parallel electric field E_{\parallel} over most of the open field except in narrow gaps along the last open field-lines (Arons 1983). The electrons accelerate and radiate from the neutron star (NS) surface to high-altitude, and emission occurs throughout the volume of the gap (Muslimov & Harding 2004; Harding et al. 2008). The OG is a vacuum gap that also forms adjacent to the last open field-line, above the null charge surface where the corotation charge (Goldreich & Julian 1969) changes sign. The gap width is determined by the screening of E_{\parallel} by pair cascades and emission occurs in a thin region along the gap inner edge (Wang et al. 2010).

Components of the magnetic field are determined from analytic expressions for the VRD (see Dyks & Harding 2004) and interpolated from numerical simulations for FFE and

resistive magnetospheres. The open field boundary on the NS surface (the PC rim) was determined via bisection in magnetic colatitude at fixed azimuth values. Open Volume radial and azimuthal Coordinates (OVC) were then defined inside the open volume of each solution (Dyks & Harding 2004). We assume that particles travel from the NS surface along open field-lines in OVCs and emit radiation tangent to field-lines, uniformly, in the corotating frame (CF). We assume that emission is also uniform across a SG of width $w = 0.05$, as a fraction of the open volume, on field-lines originating between $r_{\min} = 0.95$ and $r_{\max} = 1.0$ on the PC (in units of PC radius) and in a thin layer at $r_{\min} \simeq r_{\max} = 0.95$ in the OG. The minimum and maximum spherical radii of emission are assumed to be the NS surface and $R_{\max} = 1.2R_{\text{LC}}$, limited by a maximum cylindrical radius of $R_{\max}^{\text{cyl}} = 0.95R_{\text{LC}}$, for the SG, and the null surface and $R_{\max} = 1.5R_{\text{LC}}$, limited by $R_{\max}^{\text{cyl}} = 0.97R_{\text{LC}}$, for the OG. The photon direction is assumed to be tangent to the magnetic field in the CF, obtained through a Lorentz transformation from the inertial observer’s frame (IOF) (Bai & Spitkovsky 2010). The emission direction is then transformed to the IOF (aberration), time-delays are added and the emission is accumulated in sky-maps in viewing angle ζ and phase ϕ with respect to the pulsar rotation axis. LCs are then obtained as slices through these maps at constant ζ .

2.3. Particle Trajectory Approach

An altogether different approach to produce LCs that takes approximately into account the electric fields present in the specific magnetospheric solution is the following: Since we anticipate the velocity of any particle of the magnetosphere to be very close to c , we decompose its motion into a drift component and one parallel to the magnetic field. Thus, one can write for the particle velocity

$$\mathbf{u} = \frac{\mathbf{E} \times \mathbf{B}}{B^2}c + fc\frac{\mathbf{B}}{B} \quad (2)$$

The sign and the absolute value of the factor f is chosen so that the motion of the particle be outward and the total modulus of the velocity u be c . This trajectory determination is similar to those of Contopoulos & Kalapotharakos (2010) and Bai & Spitkovsky (2010). Under this assumption we calculate the trajectories passing through each magnetospheric point inside a central cube of edge $3R_{\text{LC}}$ considering that in the dissipative solutions the particles do not follow the field-lines in the CF. So, instead of open and closed field-lines we determine open and closed trajectories depending on whether they reach (or not) $2R_{\text{LC}}$, assuming that the radiating particles follow only open trajectories¹. This particle trajectory

¹Our field structures have E_{\parallel} in the closed zone too; we believe that this is due to approximations in our field computations and therefore we restrict radiation by particles accelerated only by the E_{\parallel} of the open

determination allows also the calculation of the local radius of curvature R_{cr} at each point of the magnetosphere. Moreover, assuming that each particle starts at the stellar surface with a small γ -value ($\gamma \lesssim 100$) we can calculate its Lorentz factor γ along its trajectory from

$$\frac{d\gamma}{dt} = f \frac{q_e c E_{\parallel}}{m_e c^2} - \frac{2}{3} \frac{q_e^2 \gamma^4}{R_{cr}^2 m_e c} \quad (3)$$

where q_e and m_e are the electron charge and rest-mass respectively. This approach allows us to have all the information needed to calculate the CR intensity contributed by each point of the magnetosphere and so the corresponding sky-maps and the LCs (see Section 2.2).

3. RESULTS

Figure 1 shows geometric LCs for SG (left-hand column) and OG (right-hand column) emission in VRD (black) and FFE (purple) solutions, and in resistive magnetospheres with $\sigma = 0.08\Omega$ (red), and 1.5Ω (green) for a range of observer angles ζ . The resistive solutions of lowest σ are closest to the VRD and indeed, the computed LCs look very similar. However, there is a shift to larger phase and a slight broadening of the peaks of the $\sigma = 0.08\Omega$ LCs. As σ increases, in both the SG and OG cases, the peaks are shifted even more to larger phase and the broadening is more pronounced, with the highest σ -value being closest to the FFE solutions. Indeed, their LCs look very similar, with only a slight shift in phase of the peaks but no further broadening. Overall, there is a distinct progression in the LC shapes as conductivity increases. The VRD LCs have the narrowest peaks and the smallest phase-lag from the magnetic pole (phase= 0), with peak-width and phase-lag systematically increasing with conductivity.

The LC changes with conductivity result from changes in magnetic field structure. Magnetospheres with low σ are “stiffer” and thus have less sweptback field-lines and smaller open field volume, while those with higher σ have more sweepback (Bai & Spitkovsky 2010). The increase of sweepback with σ produces a larger shift of the PC which causes the larger phase-lag of the LC peaks. The increase in open volume of magnetospheres with large σ also causes the increase in peak-width, since the gap widths are assumed to be a fraction of the open volume. Since peak-width and phase-lag are measurable characteristics of observed γ -ray pulsar LCs, this study shows that they could potentially be an important diagnostic of magnetospheric conductivity. Comparison of geometric LCs in VRD and FFE magnetospheres has already indicated that VRD provides a better match to observed LCs (Harding et al. 2011).

In Figure 2 we plot the LCs for solutions corresponding to three different values of σ taking into account the physical properties provided by each solution as we describe in Section 2.3. The red, green and blue color correspond to $\sigma = 0.08\Omega$, 1.5Ω , 24Ω , respectively. For these LCs we assume that emission occurs only along all open trajectories (i.e. those that reach at least up to $2R_{LC}$). The emission is considered to be due to CR and is always proportional to $\gamma^4 R_{cr}^{-2}$. The γ -value is derived by Eq. 3. The total emissivity can also be weighted by the local charge density ρ (left-hand column of Figure 2). The general feature is that the broadest (narrowest) pulses seem to be those corresponding to the middle (high) σ -value $\sigma = 1.5\Omega$ ($\sigma = 24\Omega$). However, the LCs for $\sigma = 24\Omega$ and for the low ζ -values exhibit high off-pulse emission. This effect decreases when the charge density ρ weighting is included. Moreover, near $\zeta = 90^\circ$, the middle σ -value ($\sigma = 1.5\Omega$) pulses are weak², double and narrow. The general trend for the $\sigma = 0.08\Omega$ and $\sigma = 1.5\Omega$ solutions is that the phase-lag of the pulses with respect to the magnetic poles (phase = 0) decreases with ζ although there are counter examples. These phase-lags start from values higher than 0.25 (for $\zeta = 45^\circ$) and only for ζ near 90° can reach close to 0.1-0.15. For the high σ -value ($\sigma = 24\Omega$) the corresponding phase-lags seem to be near the value 0.25 for most of the cases implying a non-monotonic behavior with σ .

We checked also the assumption that the emitting particles are mostly those that follow the high-voltage trajectories³. This approach is similar to the geometric one (Section 2.2) in the sense that it is supposed that only a part of the magnetosphere contributes to the emission. The difference here is that the active region is traced by the high-voltage trajectories. Figure 3 is similar to Figure 2 but only the 10% of the highest-voltage trajectories are considered to emit. In this case we observe narrower pulses. However, only for the middle σ -value ($\sigma = 1.5\Omega$) we have pulses corresponding to small phase-lags. We note also that the low σ -value ($\sigma = 0.08\Omega$) is observable only from a relatively narrow range of ζ ($\zeta \approx 45^\circ - 60^\circ$).

We derived also the LCs considering each point's emissivity $\propto \rho_s \gamma^4 R_{cr}^{-2}$ where ρ_s is the charge density on the star surface at the point where each particle starts its journey. In this case the results are similar to those of the right-hand columns of Figures 2, 3.

In Figure 4 we plot the points in the 3D magnetosphere that produce the pulses shown in the right-hand column of Figure 2. In each of these cases we have identified the phases of the observed pulses for all $\zeta > 30^\circ$ and we located the points that contribute over 90% of the corresponding emission. The emissivity of each point is represented by the indicated

²This is not shown in the normalized LCs of Figure 2 but only in the corresponding sky-maps.

³The voltage is given by $\int \mathbf{E} \cdot d\mathbf{l}$ along a trajectory

color scale. In these figures we have also plotted the portion of the magnetic field-lines (in gray) that contribute to the emission in the SG model presented in Figure 1. We see that there is always a blob of points over the polar caps contributing to the observed pulses. However, as we go toward high σ -values the volume of these blobs decreases and new points from the outer magnetosphere are added. For $\sigma = 0.08\Omega$ and $\sigma = 1.5\Omega$ the inner parts of the blobs coincide with only a subset of the SG lines. This subset increases with σ and at $\sigma = 24\Omega$ the largest part of the SG lines seem to follow the colored points. Beyond the light-cylinder, this region coincides with the current-sheet (Figure 4). This supports the result of (Contopoulos & Kalapotharakos 2010) where a significant part of the emission is produced near the current-sheet. The changes of the form of the effective emitting regions, described above, make the sky-maps evolution with σ complex. This makes the LCs (Figures 2, 3) evolve in a non-monotonic manner with increasing σ . However, inspection of the full sky-maps shows smooth evolution with increasing conductivity.

Figures 1-4 show that the geometric LCs are less sensitive to σ at high σ -values than those of the trajectory approach. This indicates that the E_{\parallel} distribution changes more significantly than the magnetic field structure at high σ .

4. DISCUSSION

We have presented a first implementation of dissipative magnetospheres to model pulsar emission for direct comparison with the fast accumulating pulsar phenomenology. We have concentrated here on the pulsar γ -ray LCs, however our models could also address spectral features. With LC modeling alone, we have just scratched the surface of the problem, since we have used only one of the prescriptions discussed in K12 and only one inclination angle $\alpha = 90^\circ$. A more complex behavior is expected for a variety of prescriptions and α 's.

The main goal of this paper is to show that more realistic pulsar magnetosphere models provide flexibility that allows meaningful constraints on their parameters in direct comparison with observations. While neither of the approaches employed are self-consistent in that they take into account the effects of the radiating particles on the magnetosphere itself, we find a progression in the LC shape, with peak phase and width increasing with σ in the SG and OG models. Observed Fermi LAT LCs show an inverse correlation between the peak separation Δ (in LCs with two peaks) and phase-lag δ of the first peak relative to the radio-peak (thought to be near phase = 0) (Abdo et al. 2010). The first-peak phase-lags ($\sim 0.17 - 0.2$) of high σ model LCs are too large to account for the observed δ of many LAT pulsars with $\Delta = 0.5$. The LCs computed in the particle trajectory approach can also produce narrow pulses, despite the fact that they assume particle emission at every point of

the magnetosphere; however, their consistency with observations may require specific values of ζ , α and σ . Independently of whether this is true or not, the final calculation of the LCs depends also on the modulation by the local number of the emitting particles, which is something that can be derived only in fully self-consistent solutions. We plan to move in this direction by introducing pair cascade mechanisms and the calculation of the exact particle orbits (using the full equations of motion), taking into account both CR and synchrotron losses, as well as inverse-Compton radiation.

We expect that with the dissipative models at hand, comparison of their model LC and spectral products with observations will allow us to find specific magnetospheric prescriptions and model parameters that provide the working physics of pulsar magnetospheres. All these will be the subject of future work.

AKH acknowledges support from the NASA Astrophysics Theory and Fundamental Physics Program and the *Fermi* Guest Investigator Program. We thank also the referee for his/her constructive comments.

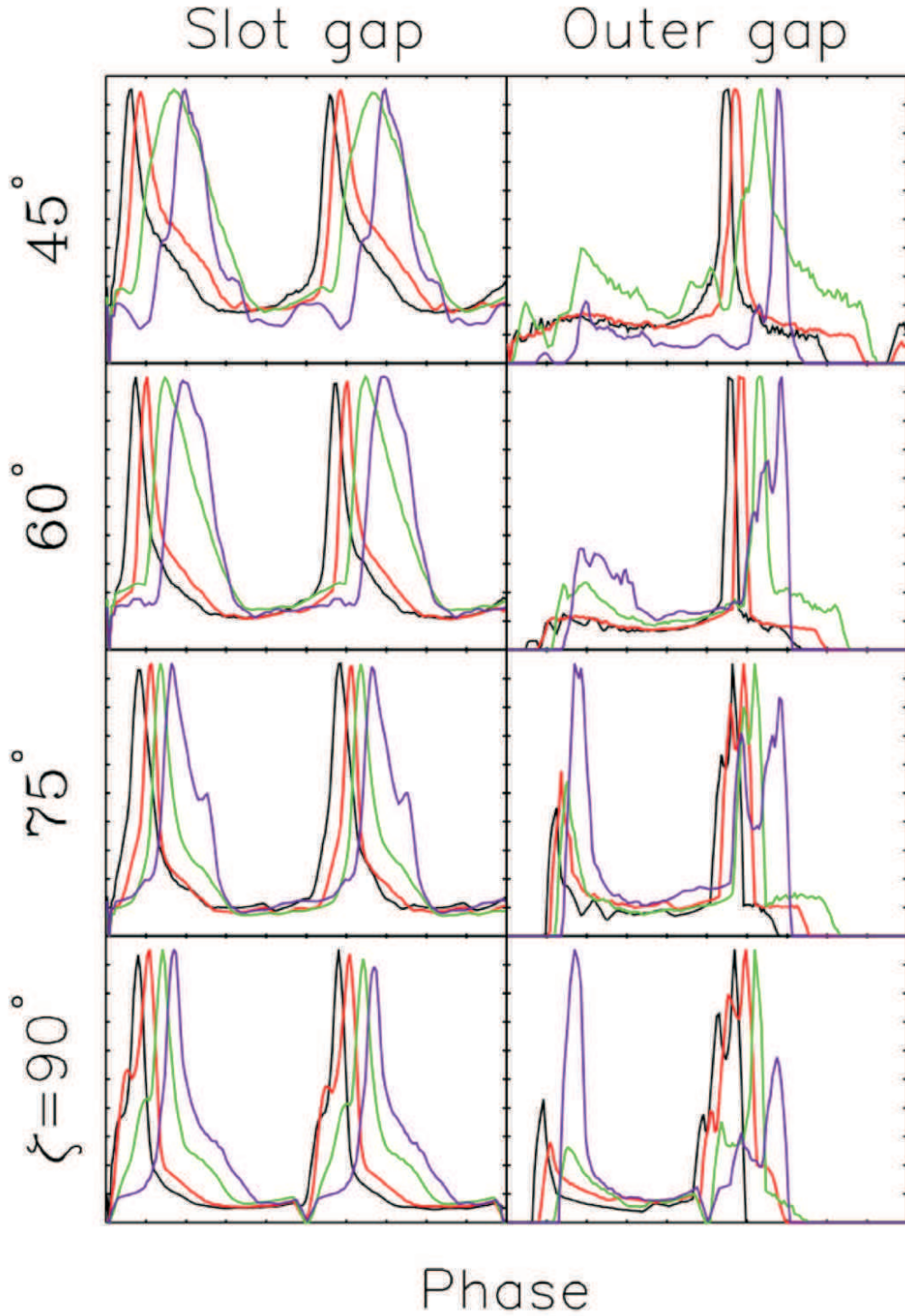


Fig. 1.— Geometric LCs for slot gap (left) and outer gap (right) emission in VRD (black), FFE (purple) solutions, and resistive magnetospheres with $\sigma = 0.08\Omega$ (red) and $\sigma = 1.5\Omega$ (green) for pulsar inclination angle $\alpha = 90^\circ$.

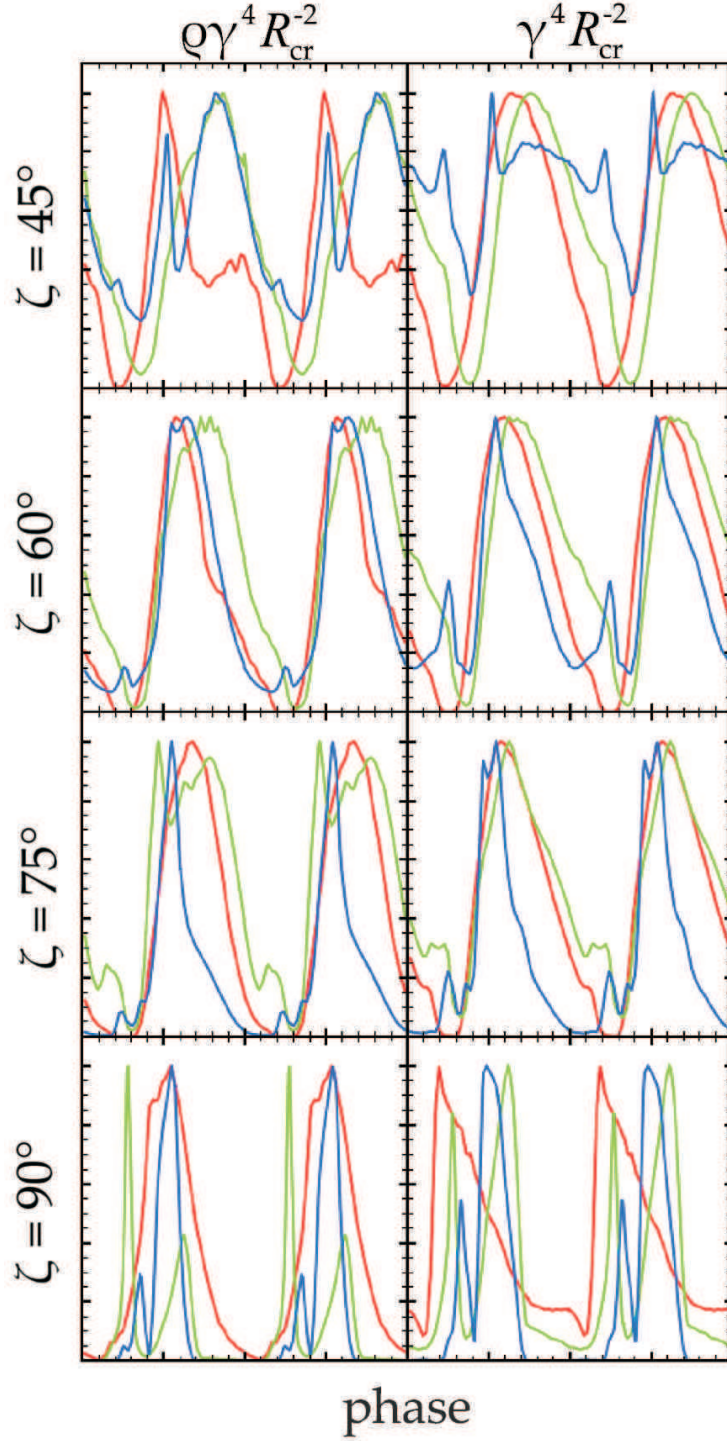


Fig. 2.— The LCs corresponding to the trajectory approach. The assumed emissivity at each point of the magnetosphere is indicated in the figure. The red, green and blue colored lines correspond to $\sigma = 0.08\Omega$, 1.5Ω and 24Ω , respectively.

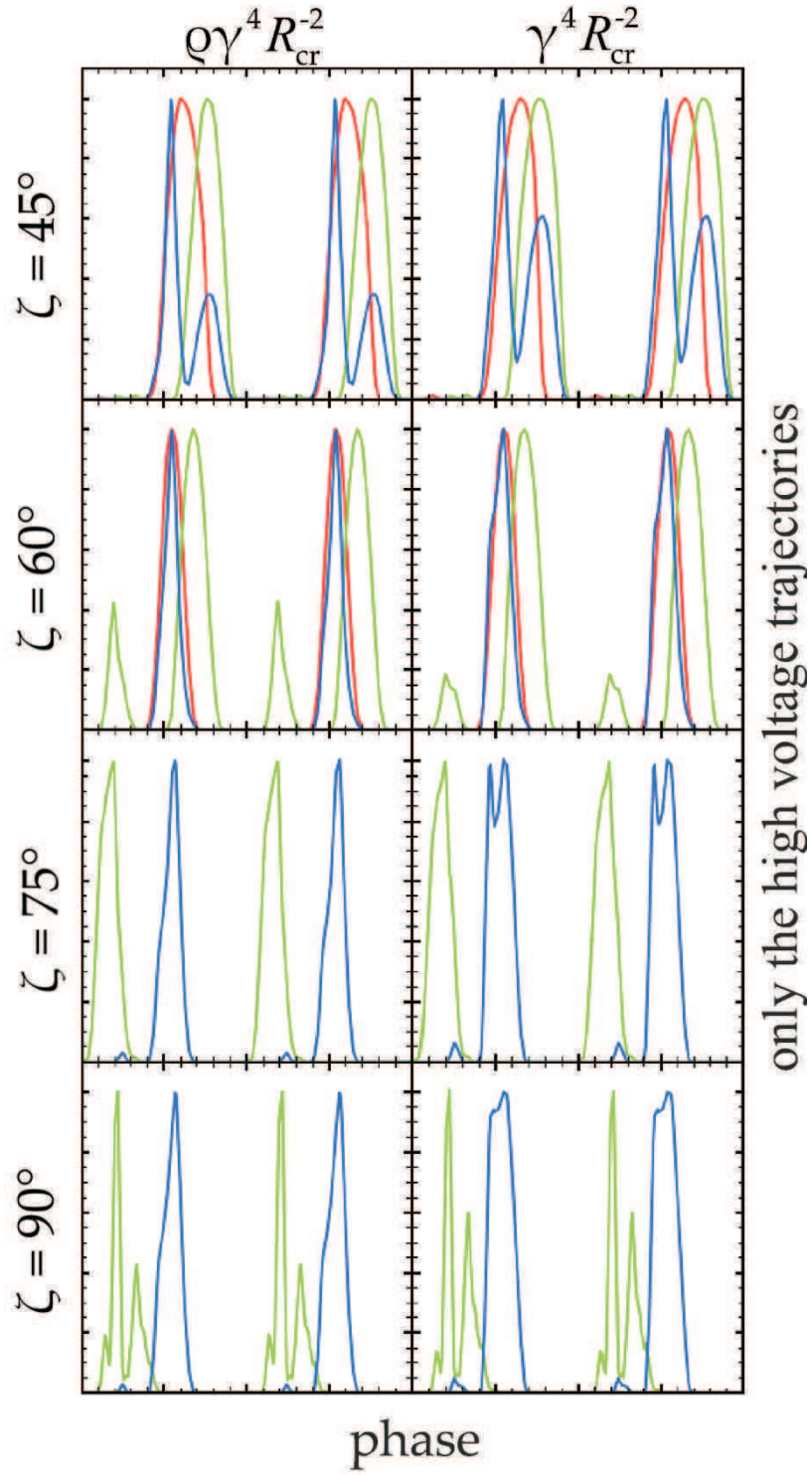


Fig. 3.— Similar to Figure 2 but only the 10% highest-voltage trajectories are assumed to emit.

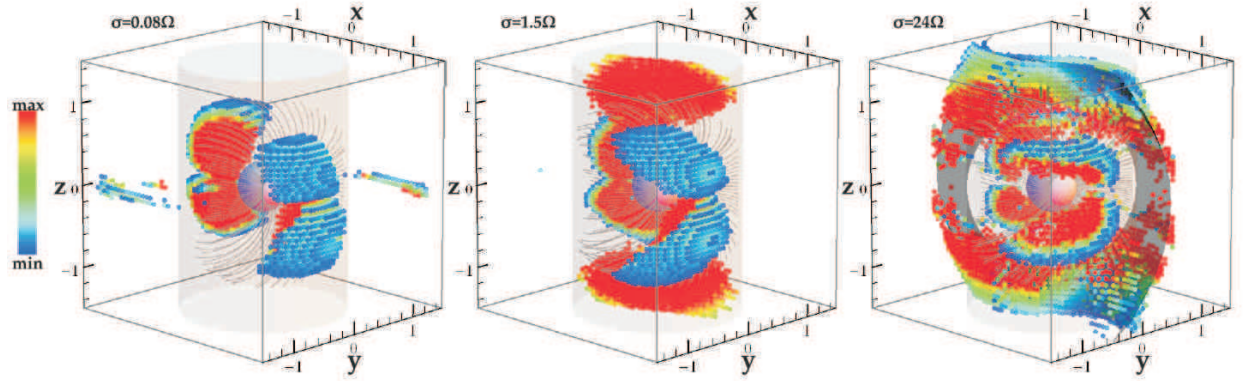


Fig. 4.— The regions of the magnetospheres that produce the peaks of the pulses shown in the right-hand column of Figure 2. The color scale indicates the corresponding emissivity. For $\sigma = 24\Omega$ a significant part of the emission comes from a region near the current-sheet outside the light-cylinder (gray surface in the right-hand panel).

REFERENCES

- Abdo, A. A., et al. 2009, *ApJ*, 696, 1084
- . 2010, *ApJSS*, 187, 460
- Arons, J. 1983, *ApJ*, 266, 215
- Bai, X.-N., & Spitkovsky, A. 2010, *ApJ*, 715, 1282
- Cheng, K. S., Ho, C., & Ruderman, M. 1986, *ApJ*, 300, 500
- Contopoulos, I., & Kalapotharakos, C. 2010, *MNRAS*, 404, 767
- Contopoulos, I., Kazanas, D., & Fendt, C. 1999, *ApJ*, 511, 351
- Deutsch, A. J. 1955, *Annales d’Astrophysique*, 18, 1
- Dyks, J., & Harding, A. K. 2004, *ApJ*, 614, 869
- Dyks, J., & Rudak, B. 2003, *ApJ*, 598, 1201
- Goldreich, P., & Julian, W. H. 1969, *ApJ*, 157, 869
- Harding, A. K., DeCesar, M. E., Miller, M. C., Kalapotharakos, C., & Contopoulos, I. 2011, [arXiv:1111.0828](https://arxiv.org/abs/1111.0828)
- Harding, A. K., Stern, J. V., Dyks, J., & Frackowiak, M. 2008, *ApJ*, 680, 1378
- Hirovani, K. 2007, *ApJ*, 662, 1173
- Hirovani, K. 2008, *Open Astronomy Journal*, [arXiv:0809.1283v1](https://arxiv.org/abs/0809.1283v1)
- Kalapotharakos, C., & Contopoulos, I. 2009, *A&A*, 496, 495
- Kalapotharakos, C., Kazanas, D., Harding, A., & Contopoulos, I. 2012, *ApJ*749, 2
- Li, J., Spitkovsky, A., & Tchekhovskoy, A. 2012, *ApJ*, 746, 60
- Morini, M. 1983, *MNRAS*, 202, 495
- Muslimov, A. G., & Harding, A. K. 2004, *ApJ*, 606, 1143
- Romani, R. W., & Watters, K. P. 2010, *ApJ*, 714, 810
- Romani, R. W., & Yadigaroglu, I.-A. 1995, *ApJ*, 438, 314

Spitkovsky, A. 2006, ApJL, 648, L51

Timokhin, A. N. 2006, MNRAS, 368, 1055

Venter, C., Harding, A. K., & Guillemot, L. 2009, ApJ, 707, 800

Wang, Y., Takata, J., & Cheng, K. S. 2010, ApJ, 720, 178

Watters, K. P., Romani, R. W., Weltevrede, P., & Johnston, S. 2009, ApJ, 695, 1289